Supporting Information

Design of Interfacial Dual Schottky Junctions to Modulate Charge Transfer for Enhanced Piezo-assisted Photocatalytic Degradation RhB Performances

Xiaoqi Jiang[a], Shengdong Sun[a], Yuqiao Wang[b]*, Lebing Zhao[a], Fangzhi Huang[a], Shikuo Li[a]*

[a]Photoelectric Conversion Energy Materials and Devices Key Laboratory of Anhui Province, Key Laboratory of Structure and Functional Regulation of Hybrid Materials (Anhui University) Ministry of Education, School of Material Science and Engineering & School of Chemistry and Chemical Engineering, Anhui University, Hefei, 230601, P. R. China.

[b]School of Chemistry and Chemical Engineering, Southeast University, Nanjing 211189, China.

*Corresponding authors. E-mail: yqwang@seu.edu.cn, hfz@ahu.edu.cn, lishikuo@ahu.edu.cn; Tel: +86-551-63861328

Catalogue

1 Materials

All chemical reagents were purchased from Sinopharm Chemical Reagent Co., Ltd, and used as received, without any further purification.

2 Experimental

2.1 *Synthesis of hollow Bi_2WO_6 nanoflower spheres*

0.97 g $Bi(NO_3)_3·5H_2O$ was dissolved in 20 mL ethylene glycol, then slowly added 20 mL 0.33 g $Na_2WO_4·2H_2O$ ethanol solution and stirred for 1 h. Transfer the mixed solution to the autoclave and keep it in 160 °C for 6 h. After cooling, the obtained samples were washed with deionized water. Afterwards, the obtained sample was calcinated at 400 °C for 1 h in air atmosphere.

2.2 *Synthesis of Bi_2WO_6@Ag*

Ag nanoparticles were deposited using photoreduction method. Specifically, 0.4 g Bi_2WO_6 was dispersed in 50 mL H_2O and 5 mL CH_3OH. Subsequently, a certain amount of $AgNO_3$ aqueous solution (1.5, 3, 4.5 mL) was added and placed under UV light for 20 min (the sample records were $BWO@Ag_{1.5}$, $BWO@Ag_3$ and $BWO@Ag_{4.5}$. Specifically, $BWO@Ag_3$ recorded as BWO@Ag).

2.3 *Synthesis of Bi_2WO_6@Ag/MXene*

Ultra-thin MXene ($Ti_3C_2T_x$) was synthesized according to the method reported in the previous literature.[1] Then, 3 mL of ultra-thin MXene solution was mixed with 50 mg Bi_2WO_6@Ag, and the sample was obtained by centrifugation after static 10 min.

2.4 *Photoelectrochemical measurements*

Photoelectrochemical (PEC) measurements were carried out in 0.5 M Na_2SO_4 solution (pH=6.8) on an electrochemical workstation (CHI 660E) with a standard three-electrode configuration (The as-prepared sample as working electrode Pt coil as counter electrode, Ag/AgCl as reference electrode). The light intensity applied during the test was 100 mW cm^{-2}. Electrochemical impedance spectroscopy (EIS) was performed by using of Zahner IM6.

2.5 *Piezo-photocatalytic activity experiments*

In this work, RhB dye molecules were selected as the target contaminants. Typically, the as-prepared 20 mg photocatalyst sample was placed in 50 mL of 10 mg L^{-1} RhB aqueous solution. Before the reaction, stir in the dark for 30 min to allow the system to reach adsorption/desorption equilibrium. Full-spectrum illumination (λ>380 nm, 100 mW cm^{-2}) and ultrasound (100 W, 40 kHz) were applied during the reaction. The degradation efficiency was evaluated by the UV absorption intensity of the solution after the reaction.

2.6 *Free radical capture experiment*

Electron spin resonance (ESR) technique was used to measure free radicals. DMPO (5,5-dimethyl-1-pyrroline-N-oxide) was selected as the trapping agent. The visible light was provided for a 300W xenon lamp (100 mW cm^{-2}). In a typical procedure, 10 mg of synthesized sample was suspended in Milli-Q water (for detection of ·OH) or methanol (for detection of ·O_2^-). Then, 10 μL of DMPO was added, and the signal was tested under dark or visible light (10 min) conditions, respectively.

2.7 *Numerical simulations*

Finite element analysis was conducted using the piezoelectric device module in COMSOL Multiphysics. To simplify the model, the diameter of the Bi_2WO_6 sphere was set to 2 μm and the thickness of the nanosheet was set to 300 nm, the diameter of the Ag particles was set to 40 nm. The MXene nanosheet was set to 500 nm. The pressure generated by bubble bursting generated by ultrasonic was set to 100 Mpa.

3 Characterization

The surface morphology and lattice structure of the samples were observed using a Zeiss Supra 40 scanning electron microscope (SEM), and JEM-2010 transmission electron microscope (TEM). The crystal structures of the sample were performed on a Philips X'Pert PRO SUPER X-ray diffractometer (XRD). The piezoelectric properties of the samples were investigated by piezoelectric response force microscopy (PFM). Elemental displacements of the samples were investigated on ESCALAB 250 Xijing X-ray photoelectron spectroscopy (XPS). The transient time resolved PL decay measurements were recorded on a FS5 fluorescence spectrometer. Elemental content was measured using the Thermo Fisher Inductively Coupled Plasma Optimization Spectrometer iCAP7400 (ICP-OES).
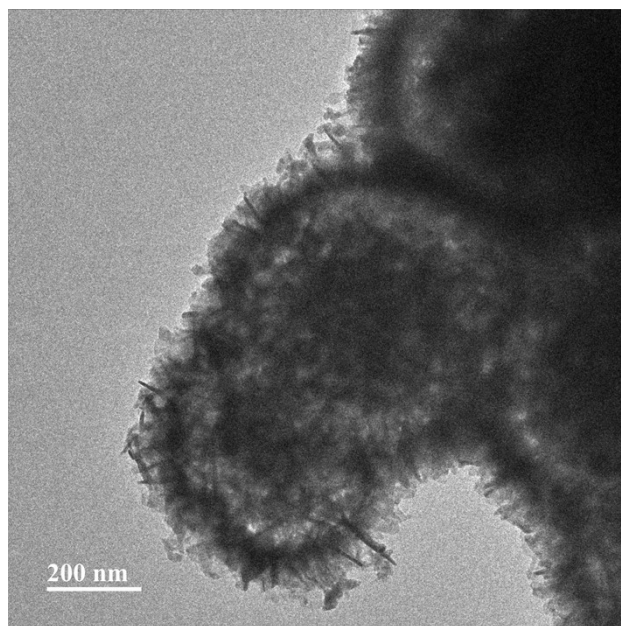
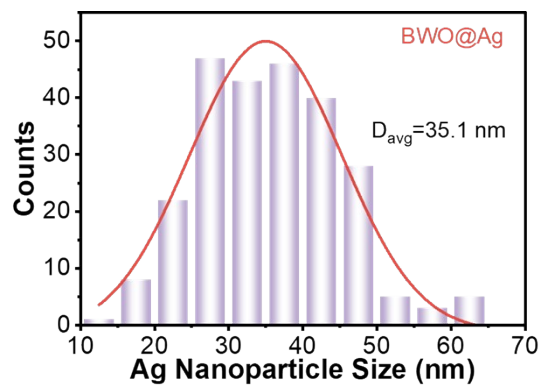# 4 Supplementary Figures

Figure S1. TEM image of Bi_2WO_6@Ag.

Figure S2. The size distribution of Ag nanoparticles.
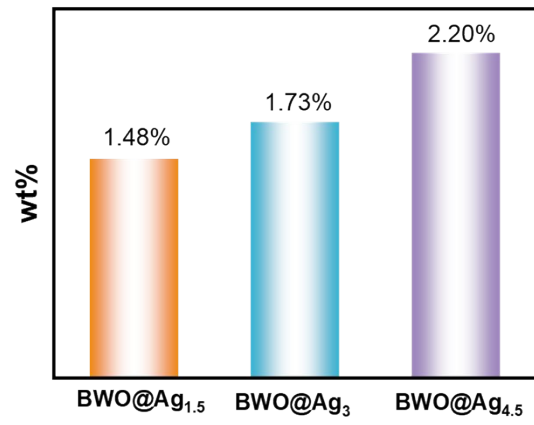
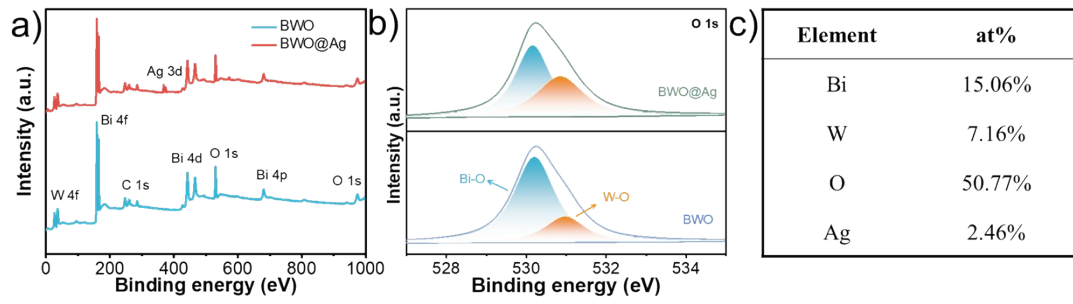**Figure S3.** ICP-OES of the BWO@Ag$_{1.5\text{-}4.5}$.

Figure S4. High resolution XPS spectra: full XPS spectra (a), O1s (b) of BWO and BWO@Ag samples. Atomic ratio of elements in BWO@Ag sample (c).
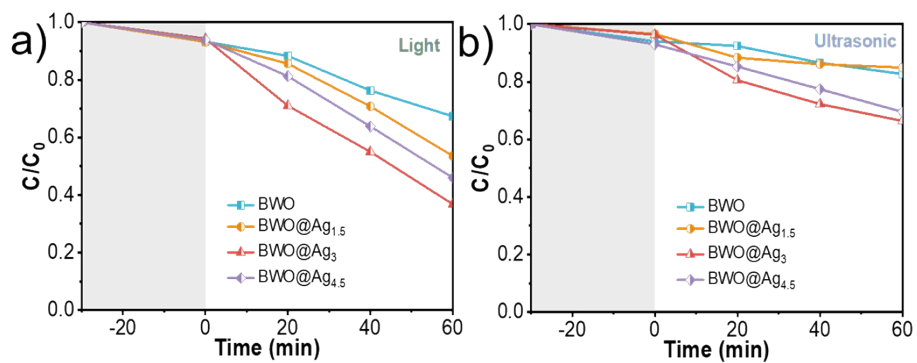
Element	at%
Bi	15.06%
W	7.16%
O	50.77%
Ag	2.46%

Figure S5. RhB degradation performance under different conditions: light illumination (a) and ultrasound (b).
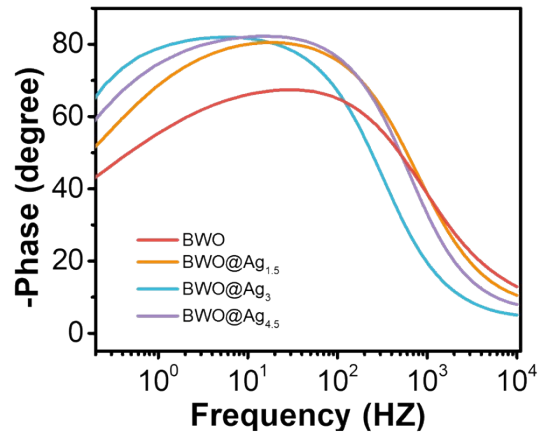
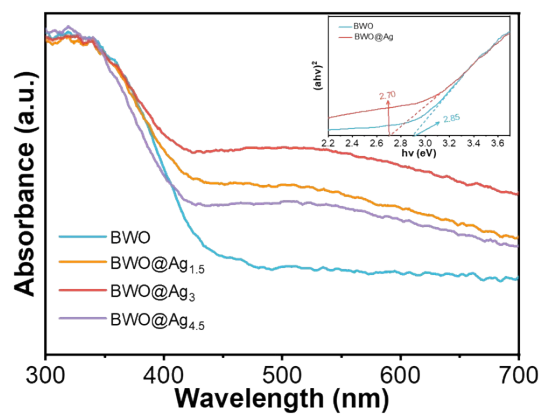**Figure S6.** Bode plot of BWO and BWO@Ag samples.
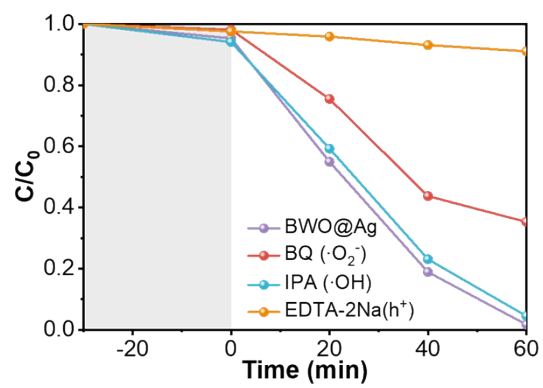
Figure S7. UV-vis spectra of BWO and BWO@Ag samples.

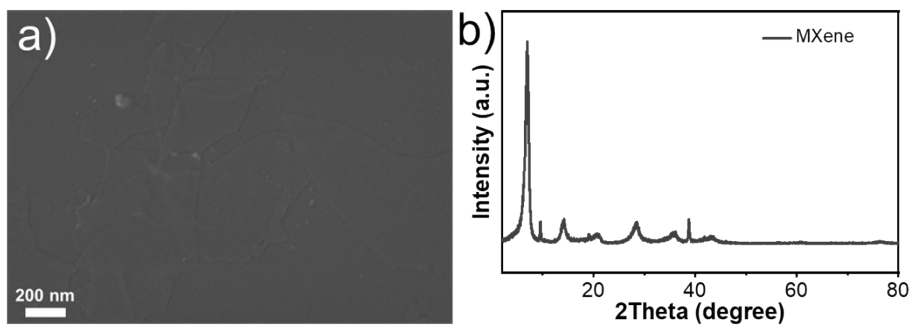**Figure S8.** RhB degradation efficiency with different capture agents.

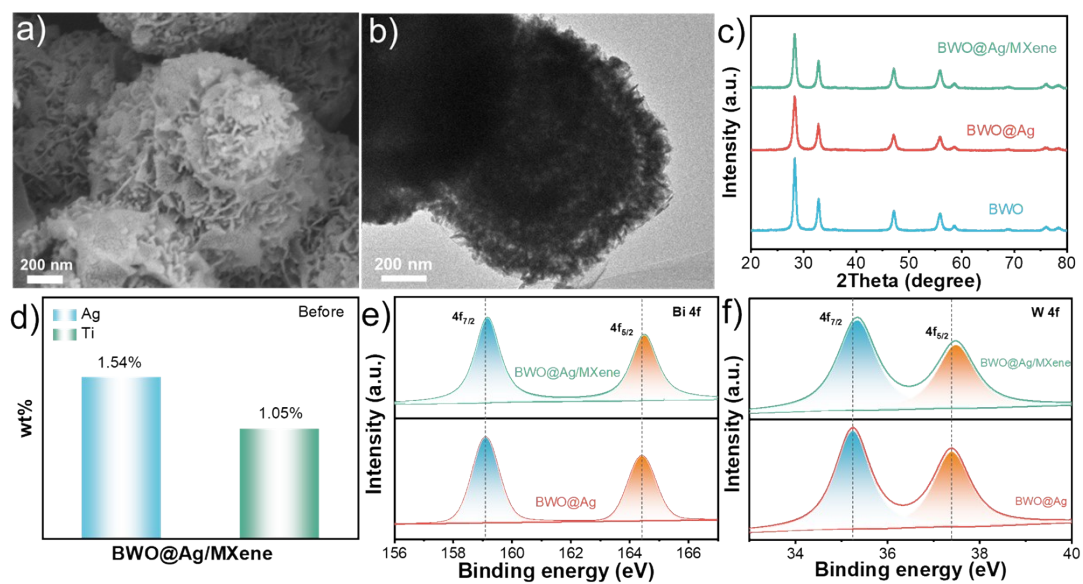**Figure S9.** SEM image (a) and XRD pattern (b) of the MXene.

Figure S10. SEM image (a), HRTEM image (b) of the BWO@Ag/MXene sample. XRD pattern (c) of the BWO, BWO@Ag and BWO@Ag/MXene samples. ICP-OES (d) of the BWO@Ag/MXene sample. High resolution XPS spectra of Bi 4f (e) and W 4f (f) for BWO@Ag and BWO@Ag/MXene samples.
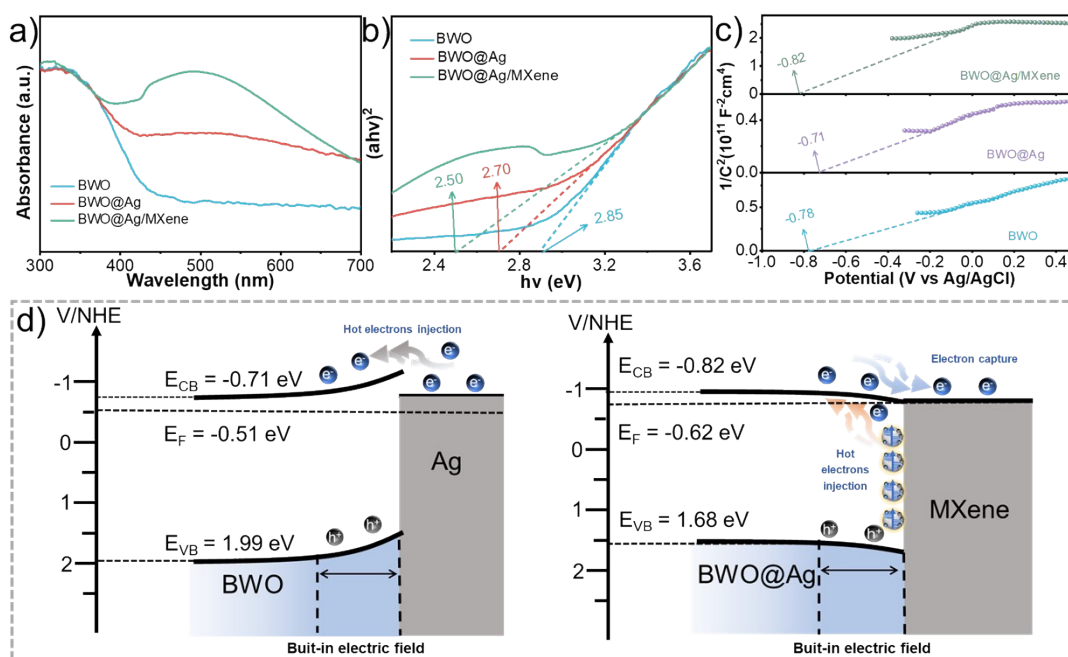
Figure S11. UV-vis spectra (a), E_g (b), M-S curves (c) of BWO, BWO@Ag and BWO@Ag/MXene. Energy band positions of BWO@Ag and BWO@Ag/MXene samples (d).

The band gaps of the samples calculated according to Figure S11a were 2.85 eV (BWO), 2.70 eV (BWO@Ag) and 2.5 eV (BWO@Ag/MXene). Meanwhile, the Fermi energy levels (E_f) calculated by M-S curve were -0.58 V *vs* NHE, -0.51 V *vs* NHE and -0.62 V *vs* NHE (Figure S11b). As shown in Figure S11c, E_f (BWO) was higher than E_f (BWO@Ag). The electrons of BWO will be transferred to Ag to balance the electron energy between the two materials. During the equilibrium process, the energy band of BWO will bend upward to form Schottky barrier (Figure S11d). Similarly, MXene has typical metal-like properties. During the electron energy balance process, the electrons of MXene will be transferred to BWO, and the energy band of BWO will bend downward to form Schottky barrier (Figure S11d).
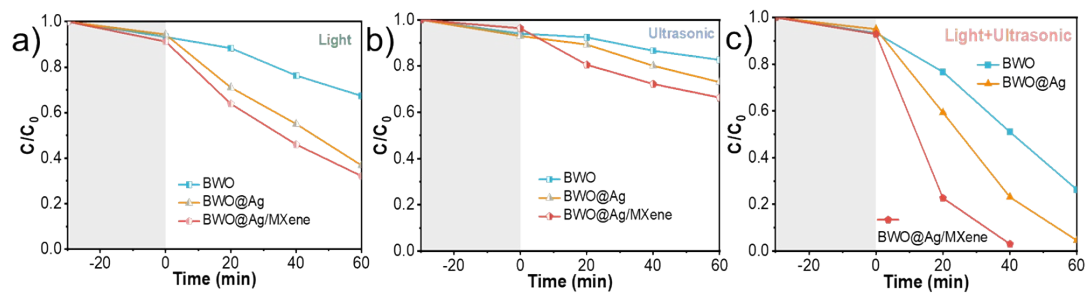
Figure S12. RhB degradation performance under different conditions: light illumination (a), ultrasound (b) and co-excitation of light illumination and ultrasound (c).
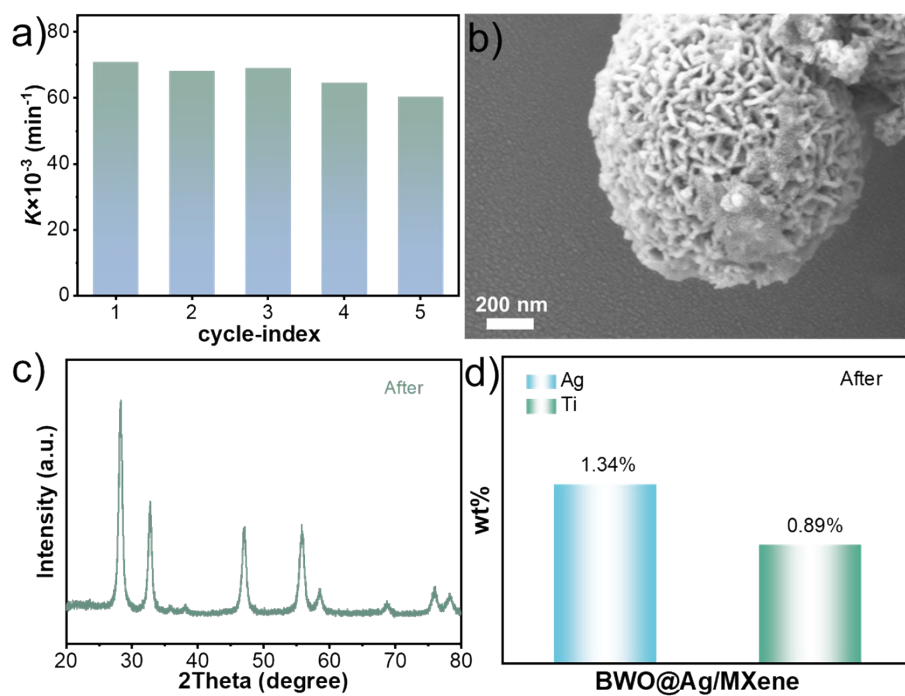
Figure S13. Corresponding *k* value within 5 degradation cycles (a), After reaction: SEM image (b), XRD (c), ICP-OES (d) of the BWO@Ag/MXene sample.
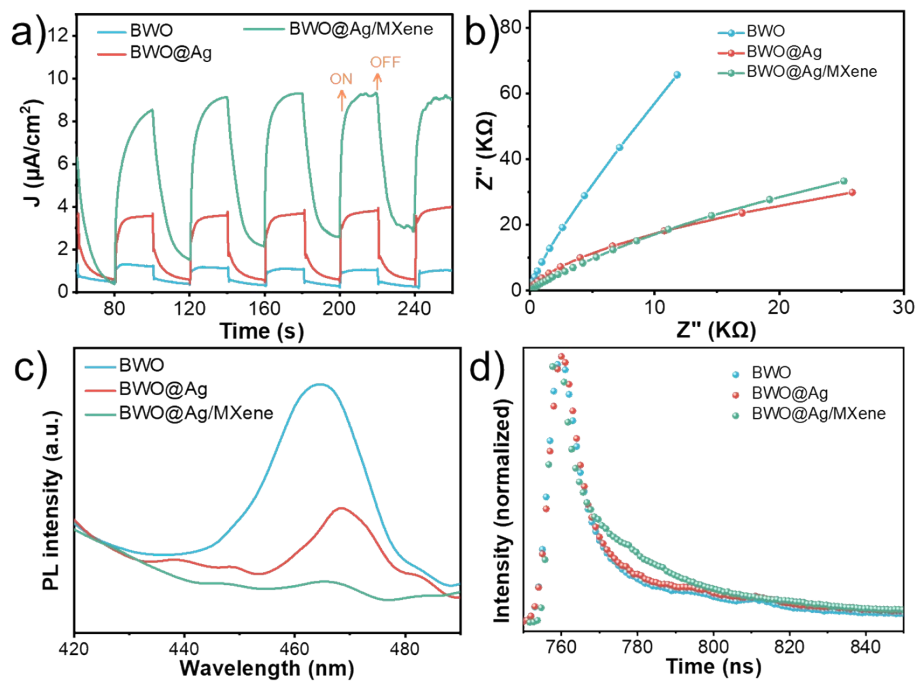
Figure S14. Transient photocurrent-time response curves (a), EIS (b), PL spectra (c), TRPL spectra (d) of the BWO, BWO@Ag and BWO@Ag/MXene.
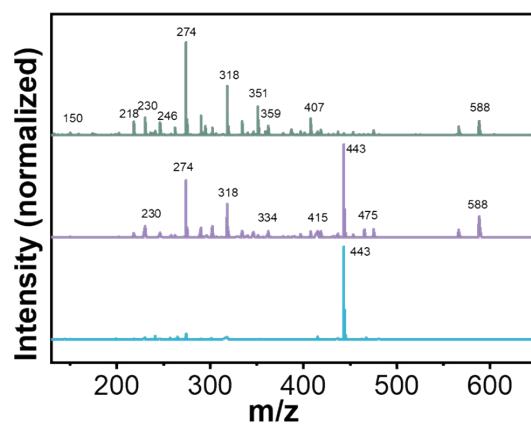
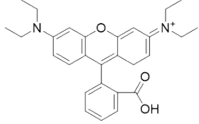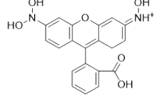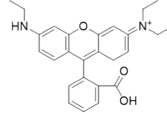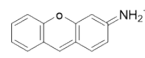**Figure S15.** LC-MS of RhB degradation intermediates.

5 Supplementary tables
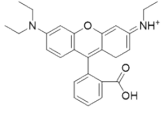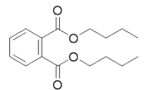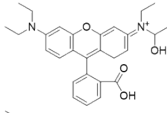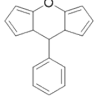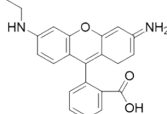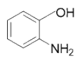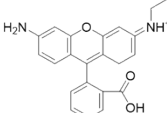
Table S1. Experimental conditions and first-order rate constants of reported piezoelectric materials.

Materials	Application	Mechanical Stress	Light	Rate constant k min^{-1}	Ref.
$KNbO_3$	50 mg photocatalyst RhB 10 mg/L 100 mL	Ultrasonic vibration 110 W, 40 kHz	300W Xe lamp	0.0222	[2]
$BiVO_4/BiFeO_3$	100 mg photocatalyst RhB 5 mg/L 50 mL	Ultrasonic vibration 180 W, 40 kHz	$\lambda > 420$ nm	0.0357	[3]
$BaTiO_3@TiO_2$	50 mg photocatalyst RhB 5 mg/L 100 mL	Ultrasonic vibration 200 W, 45 kHz	300W Xe lamp	0.08	[4]
$Bi_{0.5}Na_{0.5}TiO_3$	10 mg photocatalyst RhB 5 mg/L 100 mL	Ultrasonic vibration 200 W, 28 kHz	300W Xe lamp	0.094	[5]
$BiVO_4$:I/BTO-Ag	20 mg photocatalyst RhB 10 mg/L 50 mL	Ultrasonic vibration 150 W, 40 kHz	$\lambda > 380$ nm	0.041	[6]
$Au/AgNbO_3$	50 mg photocatalyst RhB 10 mg/L 100 mL	Ultrasonic vibration 110 W, 40 kHz	$\lambda > 420$ nm	0.054	[7]
Cl-ZnO	10 mg photocatalyst RhB 1 mg/L 50 mL	Ultrasonic vibration 100 W, 40 kHz	$\lambda > 350$ nm	0.0232	[8]
Bi_2WO_6	30 mg photocatalyst RhB 20 mg/L 60 mL	Ultrasonic vibration 120 W, 40 kHz	$\lambda = 390$ nm LED	0.077	[9]
Bi_2WO_6	10 mg photocatalyst RhB 5 mg/L 100 mL	Ultrasonic vibration 80 W, 40 kHz		0.039	[10]

Bi$_2$WO$_6$	100 mg photocatalyst RhB 10 mg/L 100 mL	Ultrasonic vibration 40 kHz		0.004	[11]
Bi$_2$WO$_6$/ZnSnO$_3$	100 mg photocatalyst RhB 10 mg/L 100 mL	Ultrasonic vibration 60 W, 40 kHz		0.035	[12]
1T@2H-MoS$_2$/Bi$_2$S$_3$	100 mg photocatalyst MB 20 mg/L 50 mL	Ultrasonic vibration 300 W, 40 kHz		0.047	[13]
Bi$_2$WO$_6$/B–TiO$_2$	20 mg photocatalyst MB 10 mg/L 60 mL	Ultrasonic vibration 240 W	220W Xe lamp	0.067	[14]
1T/2H MoSe$_2$/Bi$_2$WO$_6$	10 mg photocatalyst DCF 30 mL	Ultrasonic vibration 240 W, 40 kHz	220 V, 35W Xe lamp	~0.021	[15]
Bi$_2$WO$_6$	100 mg photocatalyst RhB, 5 mg/L 100 mL	Ultrasonic vibration 120 W, 40 kHz		0.031	[16]
MXene	10 mg photocatalyst RhB, 10 mg/L 20 mL	Ultrasonic vibration 300 W, 40 kHz		0.007	[17]
Ti$_3$C$_2$@MoS$_2$	4 g photocatalyst BPA, 10 mg/L 40 mL	Ultrasonic vibration		0.095	[18]
Ti$_3$C$_2$/SAMs-X	10 mg photocatalyst BPA, 10 mg/L 20 mL	Ultrasonic vibration 600 W, 45 kHz		0.035	[19]
g-C$_3$N$_4$/Ag/ZnO	50 mg photocatalyst RhB, 10 mg/L 50 mL	Ultrasonic vibration	LED	0.019	[20]
BiOI/BaTiO$_3$	100 mg photocatalyst RhB, 50 mg/L 100 mL	Ultrasonic vibration 180 W, 40 kHz	300W Xe lamp	0.179	[21]
Ag NPs/g-C$_3$N$_4$/Ti$_3$C$_2$	100 mg photocatalyst RhB 10 mg/L 100 mL		λ=780– 2500 nm	0.047	[22
K$_x$Ag$_{1-x}$NbO$_3$	50 mg photocatalyst RhB 10 mg/L 120 mL	Ultrasonic vibration 240 W, 40	300W Xe lamp	0.131	[23]

		kHz			
$Bi_{0.5}Na_{0.5}TiO_3@BiVO_4$	100 mg photocatalyst RhB 10 mg/L 100 mL	Ultrasonic vibration 200 W, 48 kHz	300W Xe lamp	0.045	[24]
$Au/AgNbO_3$	50 mg photocatalyst RhB 10 mg/L 100 mL	Ultrasonic vibration 110 W, 40 kHz	$\lambda > 420$ nm	0.054	[25]
$BaTiO_3@TiO_2$	50 mg photocatalyst RhB 5 mg/L 100 mL	Ultrasonic vibration 200 W, 45 kHz	300W Xe lamp	0,08	[26]
BWO@Ag/MXene	20 mg photocatalyst RhB 10 mg/L 50 mL	Ultrasonic vibration 100 W, 40 kHz	$\lambda > 380$ nm	0.072	This work

Table S2. Possible degradation intermediates of RhB.

Proposed structure	Measured (m/z)	Proposed structure	Measured (m/z)
	443		379
	415		196
	415		274
	459		230
	359		230
	359		

References

1 B. J. Wang, S. K. Li, F. Z. Huang, S. P. Wang, H. Zhang, F. H. Liu and Q. C. Liu, *Carbon*, 2022, **187**, 56-66.

2 D. F. Yu, Z. H. Liu, J. M. Zhang, S. Li, Z. C. Zhao, L. F. Zhu, W. S. Liu, Y. H. Lin, H. Liu and Z. T. Zhang, *Nano Energy*, 2019, **58**, 695-705.

3 Q. F. Jing, Z. Y. Liu, X. Cheng, C. C. Li, P. R. Ren, K. Guo, H. J. Yue, B. Xie, T. Li, Z. G. Wang and L. L. Shu, *Chem. Eng. J.*, 2023, **464**, 142617.

4 Q. Liu, D. Zhai, Z. D. Xiao, C. Tang, Q. W. Sun, C. R. Bowen, H. Luo and D. Zhang, *Nano Energy*, 2022, **92**, 106702.

5 X. F. Zhou, Q. W. Sun, D. Zhai, G. L. Xue, H. Luo and D. Zhang, *Nano Energy*, 2021, **84**, 105936.

6 X. F. Zhou, B. Shen, J. W. Zhai and N. Hedin, *Adv. Funct. Mater.*, 2021, **31**, 2009594.

7 S. Li, Z. C. Zhao, M. S. Liu, X. B. Liu, W. Huang, S. K. Sun, Y. H. Jiang, Y. Liu, J. M. Zhang and Z. T. Zhang, *Nano Energy*, 2022, **95**, 107031.

8 J. Yuan, X. Y. Huang, L. L. Zhang, F. Gao, R. Lei, C. K. Jiang, W. H. Feng and P. Liu, *Appl. Catal. B-Environ.*, 2020, **278**, 119291.

9 Z. Y. Jiang, X. J. Tan, J. Y. Xu and Y. X. Huang, *ACS Appl. Nano Mater.*, 2022, **5**, 7588-7597.

10 Z. Kang, N. Qin, E. Z. Lin, J. Wu, B. W. Yuan and D. H. Bao, *J. Clean Prod.*, 2020, **261**, 121125.

11 C. C. Lei, L. M. Song and S. J. Zhang, *Ceram. Int.*, 2020, **46**, 29344-29351.

12 C. R. Zhao, L. Y. Cai, K. Q. Wang, B. X. Li, S. D. Yuan, Z. H. Zeng, L. H. Zhao, Y. Wu and Y. M. He, *Environ. Pollut.*, 2023, **319**, 120982.

13 J. Y. Yue, R. Wu, Y. Zhang, N. Zhang, H. T. Jing, S. H. Wei and F. P. Ouyang, *Appl. Surf. Sci.*, 2023, **623,** 157033.

14 W. J. Shen, N. Li, S. X. Zuo, M. M. Wu, G. F. Sun, Q. F. Li, M. H. Shi and J. Q. Ma, *Ceram. Int.*, 2022, **48**, 15899-15907.

15 G. F. Sun, N. Li, S. X. Zuo, W. J. Shen, M. M. Wu, Q. F. Li, M. H. Shi and J. Q. Ma, *Ceram. Int.*, 2022, **48**, 37242-37252.

16 Z. H. Kang, E. Z. Lin, N. Qin, J. Wu, B. W. Yuan and D. H. Bao, *Environ. Sci.-Nano*, 2021, **8**, 1376-1388.

17 S. N. Lai, W. Y. Chen, C. C. Yen, Y. S. Liao, P. H. Chen, L. Stanciu and J. M. Wu, *J. Mater. Chem. A*, 2024, **12**, 3340-3351.

18 T. T. Ren, J. Han, Y. Miao, N. J. Li, D. Y. Chen, Q. F. Xu, H. Li and J. M. Lu, *J. Alloy. Compd.*, 2022, **925**, 166638.

19 S. X. Wang, W. R. Tian, J. Han, N. J. Li, D. Y. Chen, Q. F. Xu, H. Li and J. M. Lu, *ACS Appl. Mater. Interfaces*, 2023, **15**, 55129-55138.

20 P. P. Gotipamul, G. Vattikondala, K. D. Rajan, S. Khanna, M. Rathinam and S. Chidambaram, *Chemosphere*, 2022, **287**, 132298.

21 G. Y. Liu, H. L. Fei, Z. Feng, Q. Shao, T. Z. Zhao, W. Y. Guo and F. Li, *J. Clean Prod.*, 2024, **440**, 140886.

22 P. P. Gotipamul, G. Vattikondala, K. D. Rajan, S. Khanna, M. Rathinam and S. Chidambaram, *Chemosphere*, 2022, **287**, 132298..

23 Y. Zhang, N. N. Luo, D. Q. Zeng, C. Xu, L. Ma, G. G. Luo, Y. X. Qian, Q. Feng, X. Y. Chen, C. Z. Hu, L. J. Liu, T. Fujita and Y. Z. Wei, *ACS Appl. Mater. Interfaces*, 2022, **14**, 22313-22323.

24 Q. Liu, Q. Hu, D. Zhai, Q. W. Sun, H. Luo and D. Zhang, *J. Mater. Chem. A*, 2021, **9**, 17841-17854.

25 S. Li, Z. C. Zhao, M. S. Liu, X. B. Liu, W. Huang, S. K. Sun, Y. H. Jiang, Y. Liu, J. M. Zhang and Z. T. Zhang, *Nano Energy*, 2022, **95**, 107031.

26   Q. Liu, D. Zhai, Z. D. Xiao, C. Tang, Q. W. Sun, C. R. Bowen, H. Luo and D. Zhang, *Nano Energy*, 2022, **92**, 106702.